Scientific Research Publishing

Journal of Computer and Communications, 2026, 14(1), 145-157
https://www.scirp.org/journal/jcc
ISSN Online: 2327-5227
ISSN Print: 2327-5219

Simulation Design of Dual-Band High-Power Microwave Transmission and Radiation Antenna

Xingfu Gao, Lili Song, Linzhi Zhang, Juntao He, Yunfei Sun

College of Advanced Interdisciplinary Studies, National University of Defense Technology, Changsha, China
Email: phoezy@126.com

How to cite this paper: Gao, X.F., Song, L.L., Zhang, L.Z., He, J.T. and Sun, Y.F. (2026) Simulation Design of Dual-Band High-Power Microwave Transmission and Radiation Antenna. *Journal of Computer and Communications*, **14**, 145-157.
https://doi.org/10.4236/jcc.2026.141009

Received: December 8, 2025
Accepted: January 27, 2026
Published: January 30, 2026

Abstract

This paper aims to address the compact transmission and radiation requirements of a dual-band nested high-power microwave (HPM) source (8.4 GHz/2.0 GW at X-band, 30.6 GHz/0.9 GW at Ka-band). We have conducted simulation-based optimization on dual-band microwave support rods and a nested radiating horn. Based on the coaxial waveguide characteristics of X- and Ka-band, we used 15 dual-row support rods (spaced at $5\lambda_X/4$) and 23 dual-row rods (spaced at $13\lambda_{Ka}/4$). This enables efficient TEM mode transmission ($S_{21} > 0.99$) with a power handling capacity of 18.9 GW (X-band) and 1.4 GW (Ka-band). The radiation system has a nested design. The Ka-band undergoes mode conversion to radiate in TM_{01} mode, while the X-band is transmitted via coaxial TEM mode and then radiates in TM_{0n} mode. Simulation shows that both bands have reflection coefficients below −30 dB, with radiation gains of 19.1 dBi (X-band) and 15.8 dBi (Ka-band). The dual-frequency horn has isolation above 50 dB and meets the power handling capacity requirements. Additionally, the far-field multilobe characteristics of TE_{11}/TE_{21} modes aid experimental mode diagnosis. Overall, this design offers key technical support for compact multi-frequency HPM systems.

Keywords

Dual-Band, High-Power Microwave, Transmission, Radiation Systems, Compactness

1. Introduction

Relativistic Vacuum Electron Devices (RVEDs) generate High-Power Microwaves (HPMs) with peak powers typically exceeding 100 MW [1]-[3]. This makes them

promising for applications in military [4]-[10] and civilian fields [11]-[14], such as high-power radar [15] [16], plasma confinement [17], space energy transmission [18]-[21], and medical research. Current research focuses are shifting towards developing more practical multi-frequency output HPM sources. Compact multi-frequency HPM sources not only meet the stringent volume and weight constraints of specific platforms but also significantly compensate for the limitations of conventional single-frequency HPM sources in addressing the need to target multiple different frequencies. To achieve compact multi-frequency HPM output, researchers primarily concentrate on the design and implementation of compact multi-frequency slow-wave structures (SWS), with less attention paid to the compact design of multi-frequency HPM transmission and radiation systems. In existing research on dual-frequency transmission and radiation antennas, there are mainly two technical approaches: one is based on a single-feed horn structure [22] [23], which suffers from high transmission loss and processing difficulties; the other is based on a frequency-selective surface feed array structure [24] [25], which is typically used in satellite applications. Considering the high power capacity requirements and special application scenarios of HPMs, both of these structures are difficult to directly apply to the needs of this paper. Therefore, it is necessary to carry out simulation research on compact transmission and radiation horns suitable for dual-band HPMs.

In our previous research, a dual-band high-power coaxial transit-time oscillator (TTO) based on a nested structure was proposed, in which the Ka-band TTO was coaxially nested inside the X-band TTO. An in-depth analysis of its working mechanism and performance was conducted [26]. The typical particle simulation results are as follows: under the conditions of a voltage of 460 kV and a guiding magnetic field of 0.6 T, it can simultaneously output 2.0 GW of X-band (8.4 GHz) and 0.9 GW of Ka-band (30.6 GHz) dual-band HPM, with an average device efficiency of about 40%.To achieve simultaneous effective radiation of dual-band HPM, meet the measurement requirements of microwave experiments, and ensure the overall compactness of the dual-band HPM source, this paper combines theoretical and simulation research to carry out the compact design of the dual-band HPM transmission support rod and radiation horn.

2. Design of Dual-Band High-Power Microwave Transmission Support Rod

Due to the nested SWS design, the generation and transmission of X-band and Ka-band HPM are completed in separate spaces. Therefore, the support rods can be designed to achieve high transmission characteristics separately. The design of the support rods for coaxial TTO follows the following two principles [27]-[30]: 1) high transmission efficiency for the coaxial TEM mode (S_{21} close to 1); 2) high transmission coefficient for common low-order TE modes (such as TE_{11}) in experiments, to avoid TE mode microwaves entering the SWS and interfering with the beam-wave interaction. Existing research has shown that the selection of the

number of support rods for coaxial waveguides is based on the following criteria: near the operating frequency, when the first cutoff mode of the coaxial waveguide is the TE_{n1} mode, while ensuring low reflection for the TE_{11} mode, the number of support rods should be selected as n + 1, and they need to be uniformly distributed along the angular direction. In addition, using a double-row support rod structure with a spacing of $(2m + 1)\lambda/4$ (m is a natural number) can not only provide stronger mechanical support but also effectively broaden the transmission bandwidth of the coaxial TEM mode [27]-[29].

Using electromagnetic simulation software, the mode distribution of coaxial waveguides in the X-band and Ka-band was calculated respectively. As shown in **Figure 1**, for the X-band coaxial transmission structure, near the operating frequency of 8.42 GHz, the lowest-order cutoff mode is $TE_{14,1}$. To ensure that the TE_{11} mode also has good transmission characteristics, the number of support rods is selected to be 15. **Figure 2** shows the optimized design of the support rod model, and the structural parameters are shown in **Table 1**. The spacing between the two rows of support rods is $5\lambda_X/4$. The transmission characteristics of the support rods

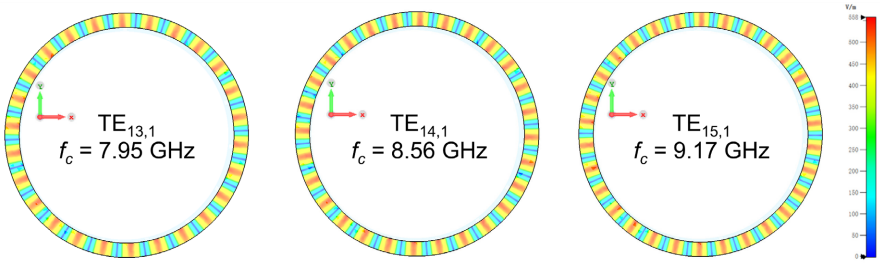

Figure 1. X-band microwave coaxial transmission channel port mode.

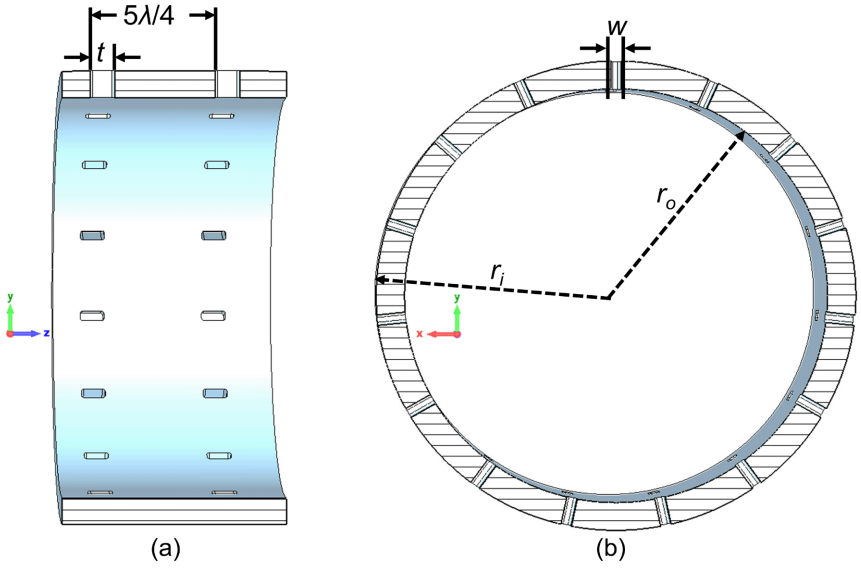

Figure 2. Cross-sections of X-band supporting rods (15 in angular direction): (a) y-z plane; (b) x-y plane.

are shown in **Figure 3**. The results indicate that the S_{21} parameter of the TEM mode is close to 1 near the operating frequency, and the S_{11} parameter of the TE_{11} mode is small, meeting the design requirements.

Table 1. Structural parameters of X-band and Ka-band supporting rods.

r_i (mm)	r_o (mm)	t (mm)	w (mm)	the first cutoff mode	number of support rods
73.1	82.9	8.8	3.7	$TE_{14,1}$	15
32.4	35.5	3.2	2.7	$TE_{22,1}$	23

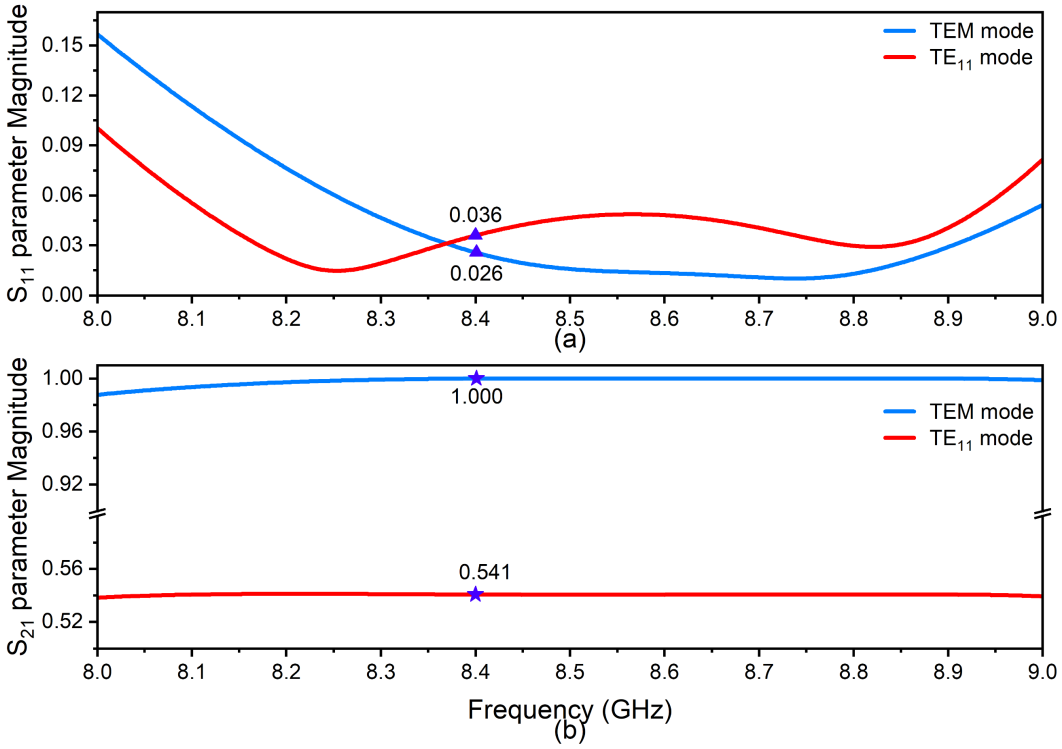

Figure 3. Transmission characteristics of X-band supporting rods: (a) S_{11}; (b) S_{21}.

The simulation results of the Ka-band coaxial transmission waveguide are shown in **Figure 4**. Near the operating frequency of 30.62 GHz, its lowest-order cutoff mode is $TE_{22,1}$. To ensure good transmission characteristics for the TE_{11} mode, the number of support rods is designed to be 23. The optimized design of the support rod model is shown in **Figure 5**, and the specific structural parameters are listed in **Table 1**. The spacing between the two rows of support rods is $13\lambda_{Ka}/4$. The transmission characteristics of the support rods are shown in **Figure 6**. The results indicate that the S21 parameter of the TEM mode is close to 1 near the operating frequency, while the S_{21} parameter of the TE_{11} mode is also relatively large. Considering that the breakdown field strength of a vacuum metal surface is 1.0 MV/cm [1], the designed power capacities of the support rods for the X-band and Ka-band are 18.9 GW and 1.4 GW, respectively, which can meet the microwave transmission requirements.

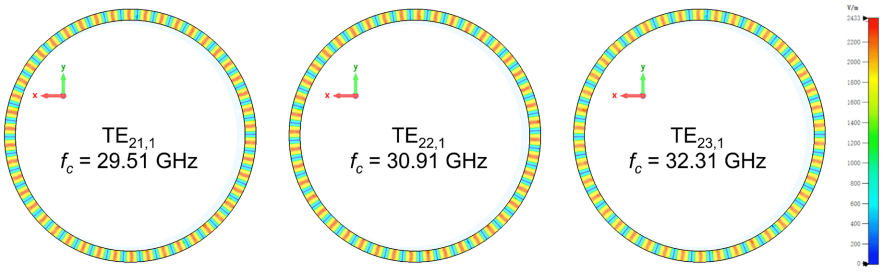

Figure 4. Ka-band microwave coaxial transmission channel port mode.

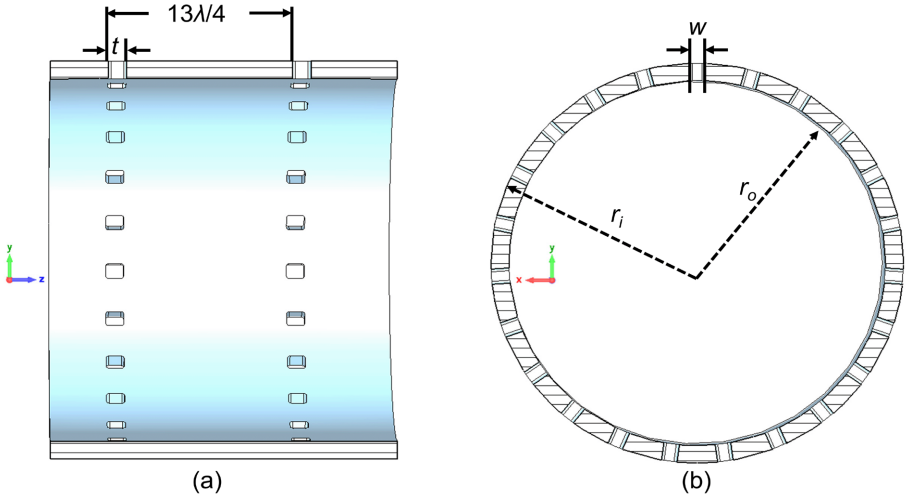

Figure 5. Cross-sections of Ka-band supporting rods (23 in angular direction): (a) y-z plane; (b) x-y plane.

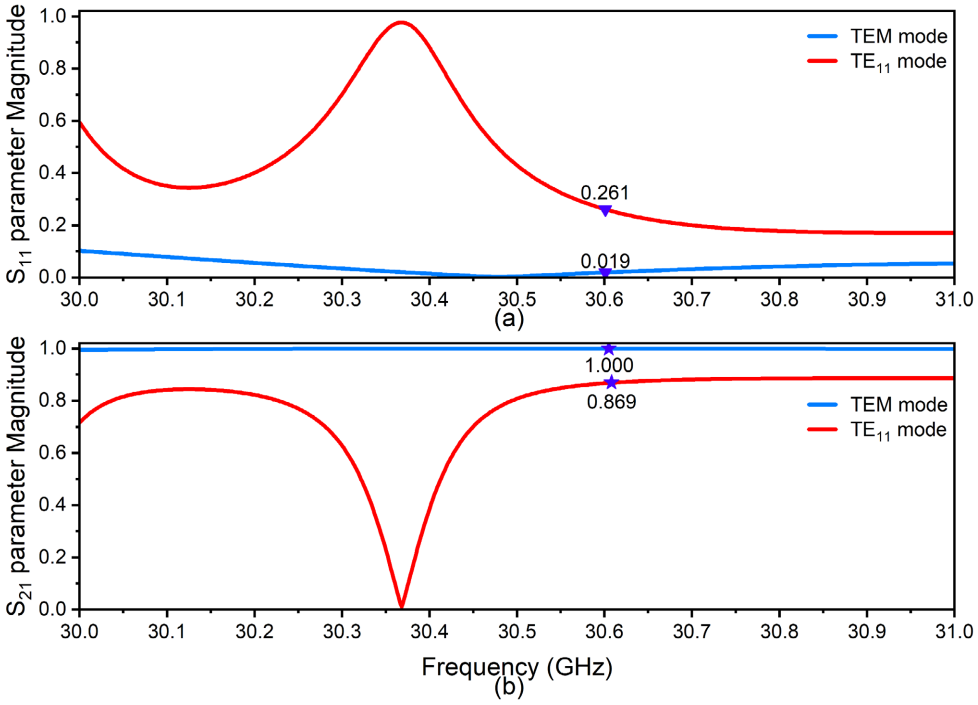

Figure 6. Transmission characteristics of Ka-band supporting rods: (a) S_{11}; (b) S_{21}.

3. Design of Dual-Band High-Power Microwave Radiation Horn

The dual-band HPM radiation horn adopts the structural configuration shown in **Figure 7**, consisting of an X-band radiation horn, a Ka-band radiation horn, and a dielectric window. In the design, by nesting the Ka-band radiation horn coaxially inside the X-band radiation horn, a compact design of the dual-band HPM radiation system is achieved, improving space utilization. There are certain differences in the radiation modes of dual-band microwaves: for Ka-band high-frequency microwaves, to reduce the risk of mode competition that may occur during transmission, a mode conversion structure is designed to convert the overmoded coaxial output channel into a less overmoded circular waveguide, achieving conversion from coaxial TEM mode to hollow TM_{01} mode and radiating outward. At the same time, the circular waveguide part of the Ka-band is designed to cut off X-band microwaves in the TM_{01} mode, so as to suppress the transmission of X-band reflected microwaves through the Ka-band transmission channel into the Ka-band slow-wave structure. Meanwhile, X-band microwaves are transmitted in coaxial TEM mode and ultimately radiate outward in TM_{0n} mode.

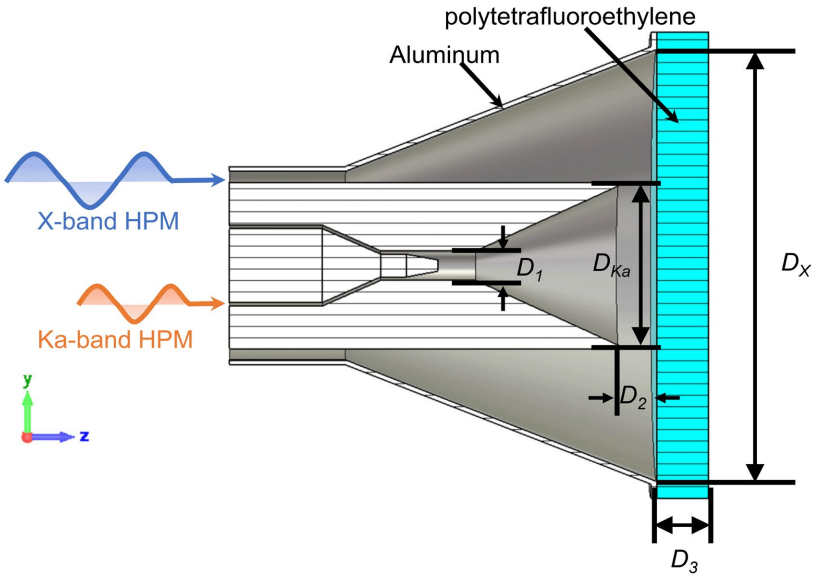

Figure 7. Schematic of dual band nested radiation antenna.

First, determine the values of the diameters D_X and D_{Ka} of the antenna radiating aperture shown in **Figure 7**. Due to the radial size limitation of the coaxial transmission channel in the X-band on the radiating horn in the Ka-band, D_{Ka} is set to 0.14 m. Meanwhile, to avoid the weight increase of the microwave source caused by the oversized dual-band radiating horn, and considering the far-field conditions of the experimental site, D_X is set to 0.38 m.

Secondly, in **Figure 7**, the value of diameter D_1 needs to not only satisfy the effective transmission of Ka-band microwaves but also ensure the cutoff characteristic for X-band reflected hollow TM_{01} mode microwaves. According to the cut-

off frequency calculation formula for TM_{mn} mode in a circular waveguide [1]:

$$f_{cmn} = \frac{u_{mn}}{2\pi r\sqrt{\mu\varepsilon}} \tag{1}$$

where u_{mn} is the nth root of the Bessel function $J_m(k_{cr})$, r is the radius of the circular waveguide, and μ and ε represent the magnetic permeability and dielectric constant, respectively. Through calculations, it is found that to make the TM_{01} mode at 8.4 GHz in the X-band in a cutoff state while ensuring effective transmission of microwaves in the Ka-band, the corresponding r should not be greater than 1.36 cm. Considering providing the highest possible power capacity for microwaves in the Ka-band, r is set to 1.3 cm, and D1 is set to $D_1 = 2r = 2.6$ cm.

The X-band and Ka-band microwaves share a common dielectric window. To ensure efficient transmission of both bands of microwaves, the reflection coefficient of the dielectric window for both bands should be as small as possible. The optimal thickness of the dielectric window can be calculated using the following formula [31]:

$$\text{Thickness} = \frac{n\lambda}{2\sqrt{\varepsilon_r}}, n = 1, 2, 3, \cdots \tag{2}$$

where λ represents the wavelength of radiated microwaves, and ε_r denotes the relative permittivity of the dielectric window material. Polytetrafluoroethylene (PTFE) is a commonly used material, with a relative permittivity value of 2.3. **Figure 8** illustrates the variation in the thickness of the dual-band dielectric window with different values of n. The results indicate that when the values of n for the X-band and Ka-band are set to 4 and 17, respectively, the required thickness of the dual-band dielectric window is approximately 47 mm, which is close for both bands. It should be noted that this value is only a theoretical reference, and the optimal thickness needs to be optimized using electromagnetic simulation software.

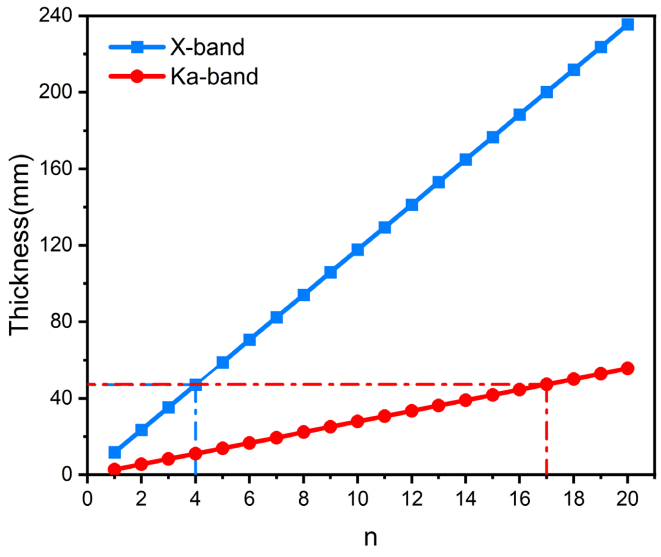

Figure 8. Calculation of the thickness of the dielectric window.

After determining the aforementioned basic parameters, the dual-band radiation horn underwent optimized design using electromagnetic simulation software. **Figure 9** illustrates the electric field distribution and three-dimensional far-field pattern when radiating X-band microwaves. It can be observed that the X-band microwaves are transmitted in a coaxial TEM mode and ultimately radiated outward in a TM_{0n} mode. **Figure 10** shows the electric field distribution and three-dimensional far-field pattern when radiating Ka-band microwaves. The Ka-band microwaves are transmitted in a coaxial TEM mode, pass through the mode converter, and are transmitted in a TM_{01} mode. Due to the gradually increasing radius of the horn, they are ultimately radiated outward in a TM_{0n} mode.

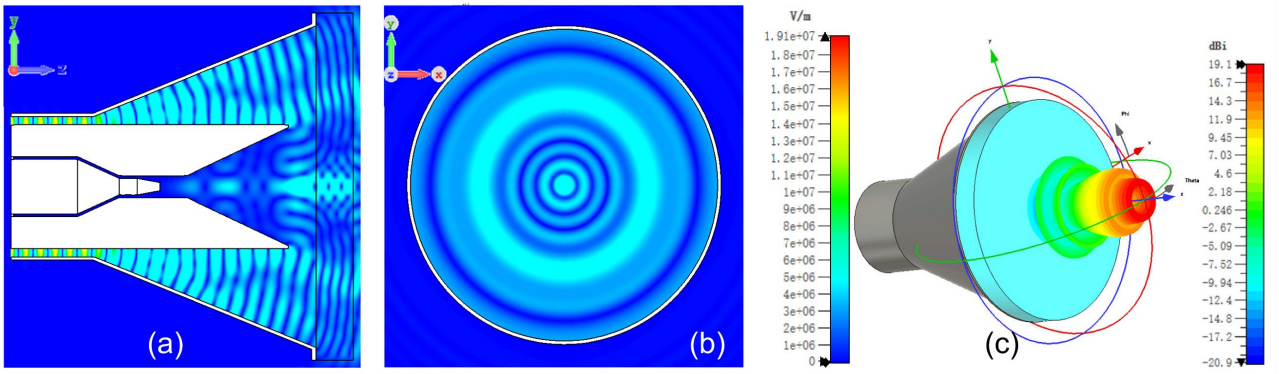

Figure 9. Electric field distribution and 3D radiation far-field pattern of radiating X-band TEM mode microwave.

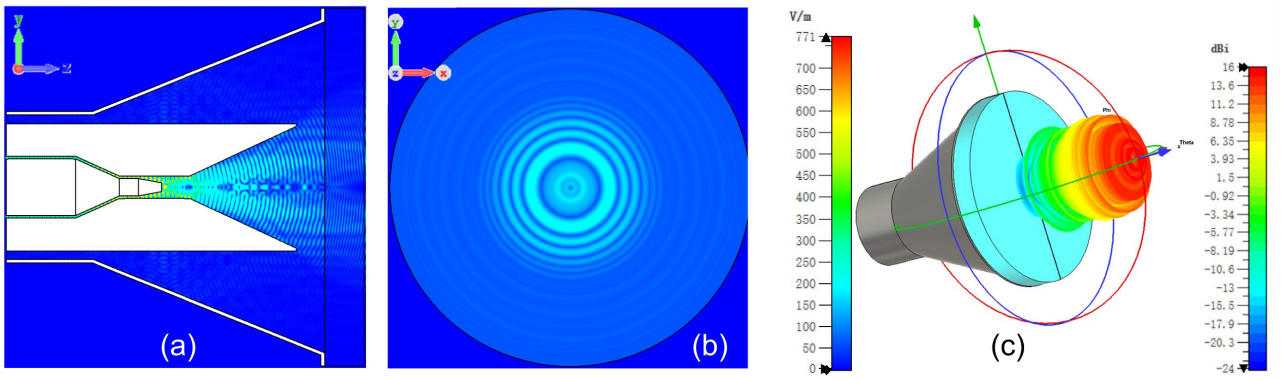

Figure 10. Electric field distribution and 3D radiation far-field pattern of radiating Ka-band TEM mode microwave.

The reflected X-band microwaves are effectively cut off in the circular waveguide section of the Ka-band mode converter. From the simulation results (as shown in **Figure 11(a)** & **Figure 11(b)**), it can be seen that the reflection coefficient S_{11} of the X-band microwaves at the operating frequency is less than −30 dB, and the radiation gain reaches its maximum value of approximately 19.1 dBi at ±8˚. Similarly, as shown in **Figure 11(c)** & **Figure 11(d)**, the reflection coefficient S_{11} of the Ka-band at the operating frequency is less than −30 dB, and the radiation gain reaches its maximum value of approximately 15.8 dBi at ±4˚. The isolation between the dual-band antennas is approximately 53.2 dB, indicating that the mutual inter-

ference between the antennas is well suppressed. When injecting 2.0 GW of microwaves, the maximum field strength on the vacuum side of the dielectric window is approximately 37 kV/cm, and the maximum field strength on the air side is approximately 29.2 kV/cm. Considering that the air breakdown field strength is 30.0 kV/cm [1], the designed dual-band horn meets the required power capacity.

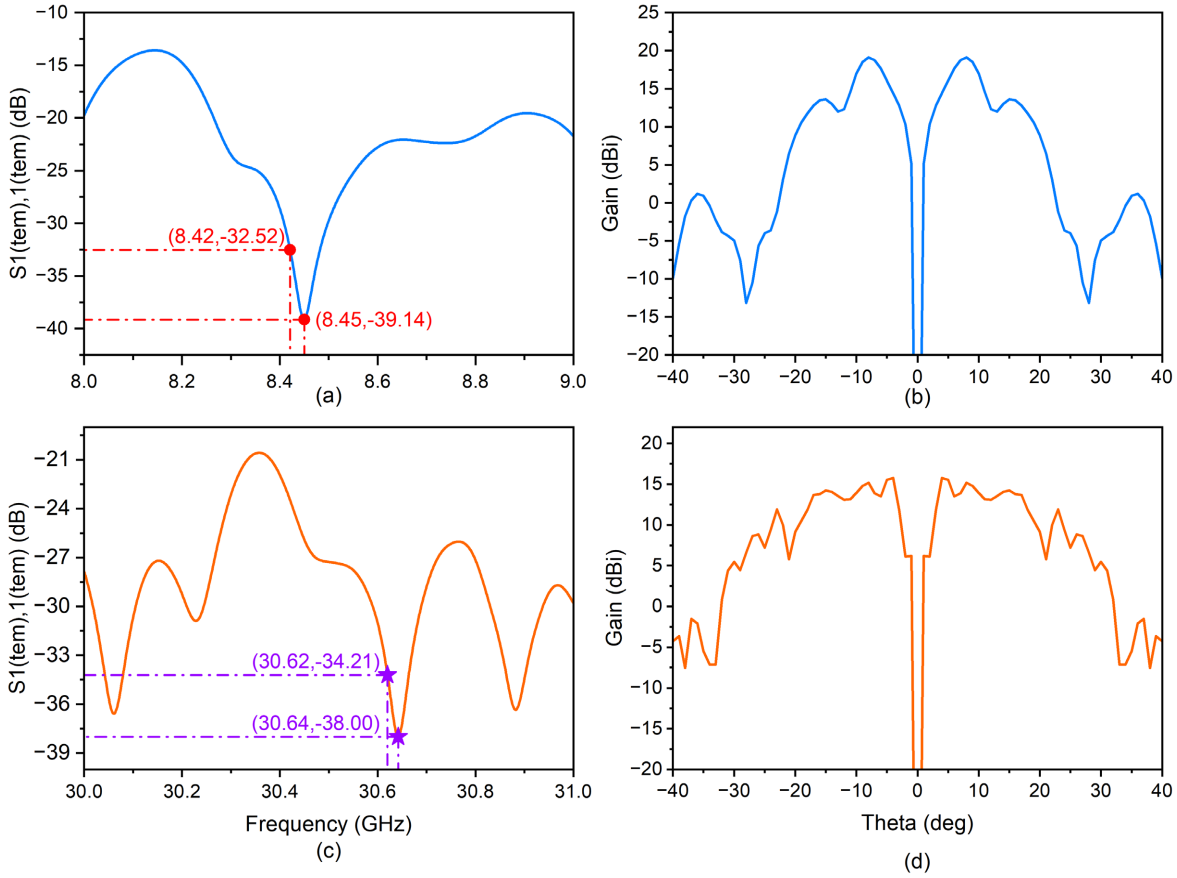

Figure 11. S_{11} parameters and 2D far-field radiation pattern: (a), (b) X-band; (c), (d) Ka-band.

In addition to ensuring that the dual-band radiating horn can efficiently radiate microwaves in the coaxial TEM mode, it is also necessary to consider the non-rotational symmetric modes (such as the common TE_{11} and TE_{21} modes) that may occur under abnormal operating conditions of the device. Therefore, in the simulation design of the dual-band radiating horn, the radiation characteristics of non-rotational symmetric modes are specifically analyzed to provide support for the identification of radiation modes and the determination of device operating states in subsequent microwave source experiments. **Figure 12** and **Figure 13** show the electric field distribution and three-dimensional radiation far-field pattern when the outer X-band horn radiates microwaves in TE_{11} and TE_{21} modes, respectively. The results indicate that after passing through a horn structure with gradually increasing radius, the TE_{11} and TE_{21} mode microwaves are transformed into higher-order modes, and their circumferential electric field distribution and

far-field radiation gain exhibit distinct multi-lobe characteristics. This is significantly different from the ring-shaped distribution of the TM_{0n} mode in **Figure 9**. This difference is helpful for identifying microwave radiation modes in microwave experiments using HPM to irradiate incandescent lamp arrays.

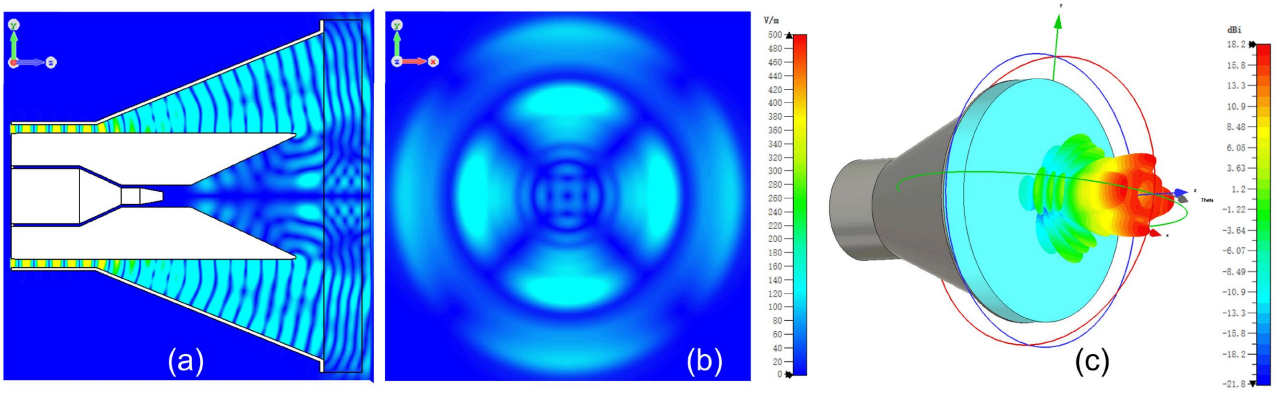

Figure 12. Electric field distribution and 3D radiation far-field pattern of radiating X-band TE_{11} mode microwave.

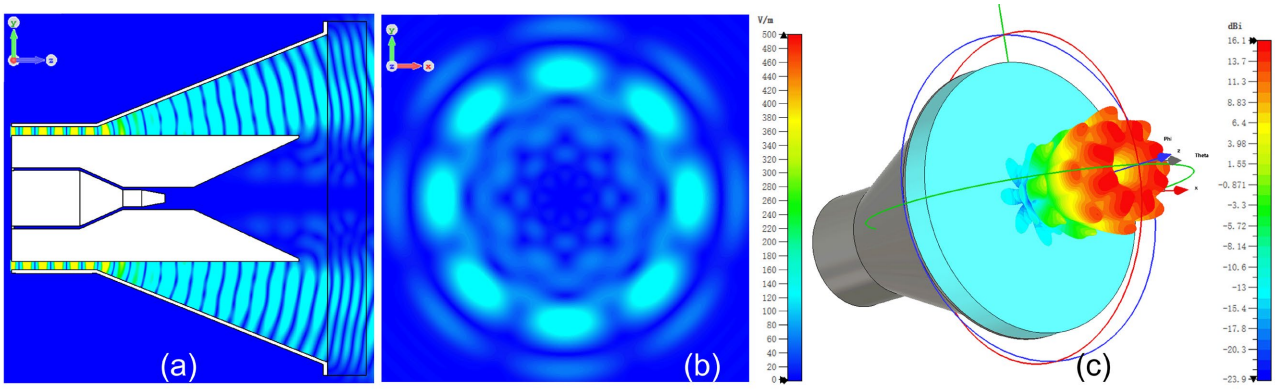

Figure 13. Electric field distribution and 3D radiation far-field pattern of radiating X-band TE_{21} mode microwave.

Similarly, **Figure 14** and **Figure 15** respectively show the electric field distribution and three-dimensional far-field radiation pattern when the inner Ka-band horn radiates microwaves in TE_{11} and TE_{21} modes. The results indicate that

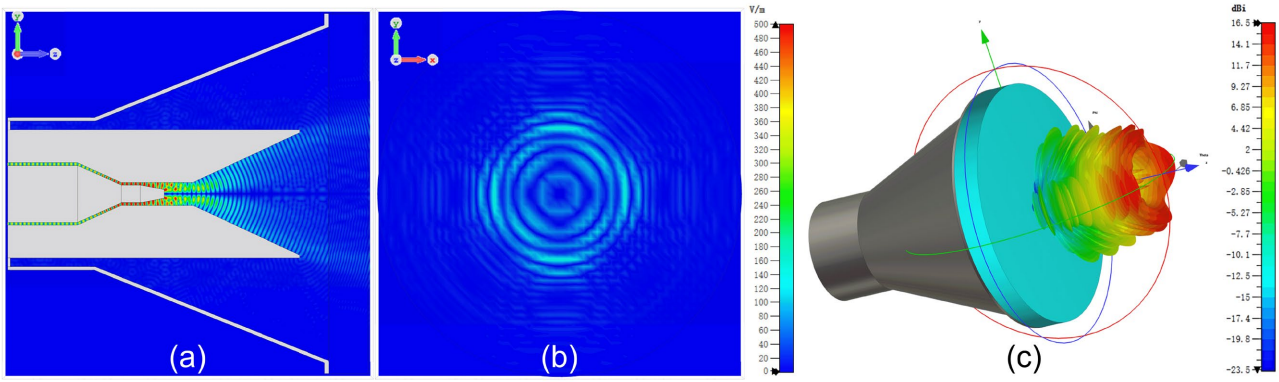

Figure 14. Electric field distribution and 3D radiation far-field pattern of radiating Ka-band TE_{11} mode microwave.

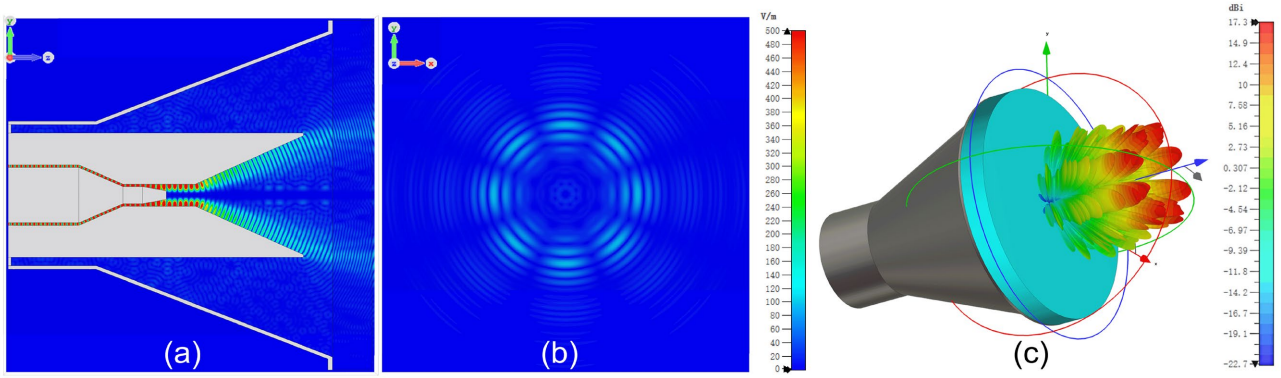

Figure 15. Electric field distribution and 3D radiation far-field pattern of radiating Ka-band TE_{21} mode microwave.

microwaves in TE_{11} and TE_{21} modes are transformed into higher-order modes after passing through the horn with gradually increasing radius, exhibiting multi-lobe characteristics in both the circumferential electric field distribution and far-field radiation gain. This multi-lobe distribution is significantly different from the circumferential ring distribution of the TM_{0n} mode in **Figure 10**, and can serve as an important basis for identifying radiation modes in experiments using HPM to irradiate incandescent lamp arrays.

4. Conclusion

This paper addresses the effective transmission and radiation of dual-band microwaves in the compact integration of X/Ka-band high-power microwave sources through the simulation and optimization design of dual-band support rods and nested radiating horns. The optimized support rods achieve efficient TEM mode transmission ($S_{21} > 0.99$) in both the X-band (15 rods, $5\lambda_X/4$ spacing) and Ka-band (23 rods, $13\lambda_{Ka}/4$ spacing). The nested radiating structure employs a differentiated mode conversion strategy, maintaining coaxial TEM transmission and radiation in the X-band as TM0n mode, while converting to TM_{01} mode for independent radiation in the Ka-band. Full-wave simulations verify that the reflection coefficients for both bands are better than −30 dB, with radiation gains reaching 19.1 dBi (X-band) and 15.8 dBi (Ka-band), respectively. The isolation between the dual-band antennas exceeds 50 dB, and the far-field multi-lobe characteristics of TE_{11}/TE_{21} modes provide a reliable basis for mode identification in experiments.

Conflicts of Interest

The authors declare no conflicts of interest regarding the publication of this paper.

References

[1] Benford, J. (2016) High Power Microwaves. 3rd Edition, Taylor & Francis Group.

[2] Kesari, V. and Basu, B.N. (2018) High Power Microwave Tubes: Basics and Trends, Volume 1. Morgan & Claypool Publishers. https://doi.org/10.1088/978-1-6817-4561-9

[3] Zhou, C.M., Liu, G.Z. and Liu, Y.G. (2007) High Power Microwave Sources. Atomic Energy Press.

[4] Wu, L.H. and Ren, Y.H. (2024) Research on Countering UAVs with High-Power Microwave Weapons. *Mobile Power & Vehicles*, **56**, 23-28+13.

[5] Meng, L., Li, T.M. and Li, H. (2015) Review of International Development of High-Power Microwaves. *Vacuum Electronics*, No. 2, 8-12+1.

[6] Qian, B.L. (2015) Research Status and Development Trends of High-Power Microwave Technology Abroad. *Vacuum Electronics*, No. 2, 2-7+1.

[7] Du, Z.B., Tang, H.R., Li, Y., *et al.* (2024) Research on Trends and Key Technologies of Air-Borne Directed Energy Weapons. *Laser & Infrared*, **54**, 1346-1351.

[8] Lan, S.Z. (2024) Accelerated Development of High-Power Microwave Weapons by the US Military. *World Affairs*, No. 13, 70-71.

[9] He, J.T., Yao, J.M. and Wang, L. (2023) Research Status and Trends of High-Power Microwave Technology in the US and Europe. *Information Countermeasure Technology*, **2**, 123-137.

[10] Li, Y.N., Wang, K., Liu, D.J., *et al.* (2024) Review of Electromagnetic Pulse Weapons Development in Foreign Militaries. *Modern Defense Technology*, **53**, 39-48.

[11] Han, C.Z., Wang, W.B., Zhao, W., *et al.* (2024) Anti-HPM Protection Design for BeiDou/GPS Navigation Systems. *High Power Laser and Particle Beams*, **36**, 1-6.

[12] Pei, J., Huang, X., Chen, S.D., *et al.* (2011) Effects of 9.33 GHz High-Power Pulsed Microwave on Proliferation of IAR20 Rat Liver Cells and L-02 Human Liver Cells. *High Power Laser and Particle Beams*, **23**, 2850-2854.

[13] Liu, S.Y. (2023) Effects of High-Power Pulsed Microwave Aging on Color and Flavor of Blueberry Wine. Master's Thesis, Shanghai Ocean University.

[14] Hang, R., Yang, X.D., Liao, Y.F., *et al.* (2022) Development of High-Power Klystrons for Large Scientific Facilities at CAS Aerospace Information Research Institute. *Vacuum Electronics*, No. 5, 14-19.

[15] Xu, J., Ren, C., Xiao, K., Chen, H. and Wu, L. (2019). High Repetition Frequency, High Power Electromagnetic Pulses Generation. 2019 *IEEE* 2*nd International Conference on Automation*, *Electronics and Electrical Engineering* (*AUTEEE*), Shenyang, 22-24 November 2019, 18-21. https://doi.org/10.1109/auteee48671.2019.9033396

[16] Jia, L.N., Wang, Y., Song, Y.X., Cui, W., Chen, Z., Wang, R., *et al.* (2024) The Detection Technology of High-Power Microwave: A Review. *IEEE Transactions on Instrumentation and Measurement*, **73**, 1-20. https://doi.org/10.1109/tim.2024.3472802

[17] Pécseli, H.L. (2020) Waves and Oscillations in Plasmas. 2nd Edition, CRC Press.

[18] Glaser, P.E. (1968) Power from the Sun: Its Future. *Science*, **162**, 857-861. https://doi.org/10.1126/science.162.3856.857

[19] Shagun, S. and Anwer, N. (2024) Space-Based Solar Power: Legal Frameworks and Sustainable Development Perspectives. *Discover Applied Sciences*, **6**, Article No. 637. https://doi.org/10.1007/s42452-024-06259-5

[20] Benford, J. (2008) Space Applications of High-Power Microwaves. *IEEE Transactions on Plasma Science*, **36**, 569-581. https://doi.org/10.1109/tps.2008.923760

[21] Caton, J.L. (2015) Space-Based Solar Power: A Technical, Economic, and Operational Assessment. UCRL-JC-106081.

[22] Flodin, J., Kildal, P. and Kishk, A. (1996) Moment Method Design of a Large S/X Band Corrugated Horn. *IEEE Antennas and Propagation Society International Symposium*. 1996 *Digest*, Vol. 3, 2030-2033. https://doi.org/10.1109/aps.1996.550006

[23] Imbriale, W.A. (2005) An Alternative Feed Design for the MRO Antenna. 2005 *IEEE Antennas and Propagation Society International Symposium*, Vol. 3A, 761-764. https://doi.org/10.1109/aps.2005.1552367

[24] Chung, M.-H. (2018) Design of a Dual-Band Feed System for S/X-Band VLBI Observations. 2018 48*th European Microwave Conference* (*EuMC*), Madrid, 23-27 September 2018, 1493-1496. https://doi.org/10.23919/eumc.2018.8541787

[25] Sushko, O., Dubrovka, R., Piltyay, S., Martyniuk, S. and Dubrovka, F. (2022) High Performance C/Ku Band Dual Polarization Feed System for 25 Meters Cassegrain Reflector Antenna. 2021 51*st European Microwave Conference* (*EuMC*), London, 4-6 April 2022, 530-533. https://doi.org/10.23919/eumc50147.2022.9784196

[26] Gao, X., Song, L., Ling, J., Peng, H., Wang, L. and He, J. (2024) High-Power X-Band and Ka-Band Microwave Generation with a Coaxially Nested Dual-Frequency Relativistic Transit Time Oscillator. *IEEE Transactions on Electron Devices*, **71**, 7802-7809. https://doi.org/10.1109/ted.2024.3471730

[27] Deng, B.F. (2021) Study on Low Magnetic Field V-Band Relativistic Transit Time Oscillator. Ph.D. Thesis, National University of Defense Technology.

[28] Cao, Y.B. (2012) Study on Novel High-Power Microwave Sources Based on Transit Radiation. Ph.D. Thesis, National University of Defense Technology.

[29] Song, L.L. (2018) Study on High-Power Coaxial Transit Time Oscillators in Ka-Band. Ph.D. Thesis, National University of Defense Technology.

[30] Ling, J.P. (2014) Study on Low Magnetic Field Coaxial Transit Time Oscillators in Ku-Band. Ph.D. Thesis, National University of Defense Technology.

[31] Wang, T. (2012) Study on Dual-Band Relativistic Backward Wave Oscillators. Ph.D. Thesis, National University of Defense Technology.